



HAL
open science

Starting the winter season: predicting endodormancy induction through multi-process modeling.

Guillaume Charrier

► **To cite this version:**

Guillaume Charrier. Starting the winter season: predicting endodormancy induction through multi-process modeling.. 2020. hal-03065757v1

HAL Id: hal-03065757

<https://hal.inrae.fr/hal-03065757v1>

Preprint submitted on 14 Dec 2020 (v1), last revised 24 Nov 2021 (v3)

HAL is a multi-disciplinary open access archive for the deposit and dissemination of scientific research documents, whether they are published or not. The documents may come from teaching and research institutions in France or abroad, or from public or private research centers.

L'archive ouverte pluridisciplinaire **HAL**, est destinée au dépôt et à la diffusion de documents scientifiques de niveau recherche, publiés ou non, émanant des établissements d'enseignement et de recherche français ou étrangers, des laboratoires publics ou privés.

Starting the winter season: predicting endodormancy induction through multi-process modeling.

Guillaume Charrier¹

¹Université Clermont Auvergne, INRAE, PIAF, 63000 Clermont-Ferrand, France

*: corresponding author

Email: guillaume.charrier@inrae.fr

Tel: +33 4 43 76 14 21

UMR PIAF, INRAE Site de Crouel

5, chemin de Beaulieu

63000 Clermont-Ferrand

1 **Abstract**

2 In perennial plants, the annual phenological cycle is subdivided into successive stages whose
3 completion will lead directly to the onset of the following one. A critical point is the transition
4 between the apparent vegetative growth and the cryptic dormancy. To date, the initial date for
5 chilling accumulation (D_{CA}) is arbitrarily set using various rules such as fixed or dynamic dates
6 depending on environmental variables. These rules led to tremendous variability across studies
7 and sites (from late summer until late autumn). To test the relevancy of different D_{CA} , we used
8 a dataset combining dormancy release dates, budburst dates and frost hardiness measurements
9 from 50 years in various orchards across France and Spain for *J. regia* cv Franquette. Many of
10 the tested D_{CA} provided accurate results for the calibration and validation datasets ($RMSEP <$
11 10 and 8 days for endodormancy release and budburst dates, respectively). However, for frost
12 hardiness, only the D_{CA} provided by the DORMPHOT model provided accurate results
13 ($RMSEP < 3^{\circ}C$). The best D_{CA} was thus selected using a composite index for all three processes.
14 Testing the prediction under current and future climatic scenario showed that in, up to 25% of
15 French territory under RCP 8.5 scenario, ecodormancy stage is likely to be delayed although
16 temperature is decreasing. Overall, less average frost damages are expected although decennial
17 risk (*i.e.* return period of ten years) is likely to increase in autumn in 15% of French territory.
18 In southern part of France, delayed dormancy induction and release would induce delayed
19 budburst and blooming altering flower and fruit production, whereas North East and Massif
20 Central parts of France may suffer higher frost risks from late frost acclimation. Finally, this
21 study describes relationships between climatic variables and plant phenological processes to
22 build metamodels predicting next century's phenological cycles at the global scale.

23

24 **Keywords:** Chilling, Frost acclimation, Frost damages, Forcing, Photoperiod, Phenology, Risk
25 assessment, Tree.

26 **Introduction**

27 In frost-exposed environments, deciduous trees have to timely adjust their biology and
28 increase frost resistance by anticipating unfavorable conditions before the winter period. As
29 observed for most stresses, avoidance and tolerance are two complementary processes driving
30 frost resistance (Charrier *et al.*, 2011). The protection of shoot apical meristems under bud
31 scales can be considered as an avoidance strategy. This is achieved through physiological
32 changes allowing the transition from an apparently active (*e.g.* primary and secondary growth,
33 leaf expansion, fruit maturation) towards a ‘dormant’ period (*e.g.* endodormancy and
34 ecodormancy; Lang *et al.*, 1987). During this transition, different phenologically-related
35 processes that are either visible (*e.g.* leaf fall, growth cessation, lignification or budset) or
36 invisible (*e.g.* dormancy induction and release) take place. In parallel, trees transiently increase
37 their frost tolerance through frost acclimation / deacclimation process (Charrier *et al.*, 2011).

38 In autumn, endodormancy release and frost acclimation are induced by the same
39 environmental factors, namely decreasing temperature and photoperiod (Welling *et al.*, 2002;
40 Arora *et al.*, 2003; Maurya & Bahlerao, 2017). After endodormancy was released, ecodormancy
41 and frost deacclimation also occurs in parallel, under the control of warm temperature, in most
42 species, eventually modulated by photoperiod in photosensitive species, such as late
43 successional species (Basler & Körner, 2012). Process-based models using these variables as
44 input have been developed to simulate the dormancy release and budburst dates (Chuine *et al.*,
45 2016), as well as frost hardiness (*e.g.* Leinonen 1996; Ferguson *et al.*, 2011; Charrier *et al.*,
46 2018).

47 Under the context of global change, it is particularly critical to accurately predict future
48 trends in warmer climates. Since the first empirical model describing the relation between
49 temperature and plant development, through the thermal-time concept (Réaumur, 1735),
50 budburst and blooming models were only computing accumulation of growth-effective

51 temperature *i.e.* growth degree days (GDD). As the starting point was set at the coldest period
52 of the year (*i.e.* January 1st or July 1st in northern and southern hemisphere, respectively), these
53 models provided accurate results. However, this type of model was not efficient under warmer
54 winter areas, where temperate crop species were attempted to grow (*e.g.* Northern Africa,
55 Middle East or South America; Balandier *et al.*, 1993). In this context, temperate perennial
56 crops did exhibit lack of chilling and insufficient endodormancy release (Weinberger, 1950).
57 The process of endodormancy, and related chilling accumulation, had thus been introduced into
58 models (Weinberger, 1956; Vegis 1964). In the recent decades, naturally growing trees have
59 also been affected by a reduction in chilling exposure throughout winter, enhancing the interest
60 into the endodormancy stage (Gauzere *et al.*, 2019).

61 Two-step models, simulating endo- and ecodormancy stages, are now commonly used to
62 predict budburst dates (Chuine *et al.*, 2016). Frost acclimation models use similar formalism
63 with direct linkage between frost acclimation and exposure to chilling temperatures followed
64 by frost deacclimation and exposure to forcing temperatures, respectively. In perennial plants,
65 the completion of a stage will directly drive the onset of the following ones (Hänninen &
66 Tanino, 2011). However, the initial date for chilling accumulation (D_{CA}) is usually arbitrarily
67 set with various rules leading to tremendous variability across studies (from late summer until
68 late autumn). Four different concepts of D_{CA} have been used (see Tab. S1):

- 69 - Fixed date across years and locations: from September 1st (Chuine *et al.*, 2016) until
70 November 1st (Weinberger, 1967), for northern hemisphere,
- 71 - Dynamic date through a simple climatic threshold: critical temperature (*e.g.* date of the first
72 frost; Landsberg, 1974) or photoperiod (Welling *et al.*, 1997),
- 73 - Dynamic date through a mathematic function using a single variable such as the date of
74 minimum chilling units computed by the Utah model (Richardson *et al.*, 1974),

75 - Dynamic date through a mathematic function using interacting variables (temperature and
76 photoperiod) simulating leaf fall date (Delpierre *et al.*, 2009) or dormancy induction
77 (DORMPHOT; Caffarra *et al.*, 2011a).

78 These different approaches have mainly been used for phenological cycle prediction. Thanks
79 to a large dataset combining data from 50 years in various orchards across France and Spain for
80 *J. regia* cv Franquette, we tested different formalism to compute the effects of the onset of
81 chilling accumulation D_{CA} on the accuracy of three related processes (endodormancy,
82 ecodormancy and frost acclimation/deacclimation). The optimal model was subsequently
83 assessed for future climate prediction over France following three contrasted *scenarii*.

84 **Material and methods**

85 *Endodormancy release and budburst dates*

86 Endodormancy release dates were measured using the one-node-cutting ‘forcing’ test of
87 Rageau (1982). Samplings were performed every three weeks from October until May and 48
88 one-node cuttings prepared per sampling date. Buds were isolated from other parts of plant to
89 prevent correlative inhibitions (Dennis, 2003). At each sampling date, one-year-old stems were
90 cut in 7-cm long pieces, bearing only one node at the top or less than 1 cm below the top end,
91 for terminal and axillary buds, respectively. For axillary buds, the top of the cutting was covered
92 by paraffin wax to prevent desiccation. The bases of the cuttings were immersed into tap water,
93 weekly changed. Cuttings were exposed to optimal conditions for growth resumption (*i.e.* 16/8
94 D/N and 25°C) and individually observed every 3 days. Mean time until budburst (stage 09
95 BBCH) were computed from individual time until budburst for each cutting. After
96 endodormancy release, buds of *J. regia* cv Franquette break out after 20 days under optimal
97 conditions (Mauget, 1980; Charrier *et al.*, 2011). Endodormancy release dates were thus
98 obtained by linear interpolation between the two dates giving a time to budburst higher (or equal

99 to) and lower (or equal to) than 20 days, respectively. Budburst in the field was monitored every
100 two to three days in the different sites until 50% of buds reached the stage 09 of the BBCH
101 scale.

102 *Frost hardiness*

103 Frost hardiness was measured from September until budburst on one-year-old branches in
104 different orchards (Tab. 1) using the electrolyte leakage method (Charrier & Améglio 2011).
105 Samples were cut into six 7-cm-long segments without buds and exposed to four different
106 freezing temperatures among this set of temperatures: -5, -10, -15, -20, -30 and -40 °C.
107 Depending on the season, either the highest or the lowest temperatures were not used. Two
108 supplementary subsamples were exposed to control (+5 °C) and maximal freezing temperature
109 (-80 °C). Freezing and thawing rates were set to 5 K h⁻¹.

110 Relative electrolytic leakage (REL) was calculated as (C1/C2) as described in Zhang &
111 Willison (1987). We assumed a sigmoidal relationship between REL and temperature (θ) for
112 each sample:

$$113 \quad REL = \frac{a}{1+e^{b(c-\theta)}} + d \quad (1)$$

114 where parameters a and d define asymptotes of the function, and b is the slope at the inflection
115 point c.

116 Frost hardiness was defined as the temperature of the inflection point (c) of the adjusted logistic
117 sigmoid function (Repo & Lappi 1989), whereas frost sensitivity was considered to be estimated
118 by the parameter b in percent damage per Celsius degree.

119 *Climate data*

120 Models were fit using observed daily mean and minimal temperature monitored by weather
121 station, located most of the time in the same orchard and closer than 10km distance (Table 1).

122 For predictive purpose, the temperature, calculated according to the CNRM-ALADIN52 model
123 and corrected by a Q-Q method (Déqué *et al.*, 2007), were used from 8462 sites across France
124 (Safran grid at 8km spatial resolution; MétéoFrance). Four datasets were used as input variable:
125 reference period (1950-2005) and three contrasted climatic *scenarii* (RCP 2.6, RCP 4.5 and
126 RCP 8.5) for the future period (2005-2100). For each site and day, day and night length were
127 computed depending on the latitude and day of year.

128 *Endodormancy induction and onset of chilling accumulation*

129 Date of the onset of chilling accumulation (D_{CA}) was computed through different functions:

130 i) Fixed D_{CA} every *ca.* 10 days from DOY 182 (July 1st) until DOY 335 (November 30th).

131 ii) Dynamic D_{CA} based on threshold values reached by minimum temperature (T_{min}), mean
132 temperature (T_{mean}), first frost (FF) or photoperiod.

133 iii) Date of minimum chilling units (CU_{min}) were computed according to the Utah model
134 (originally developed on *Prunus persica*) that computes negative chilling effect for
135 temperature higher than 16°C (Richardson *et al.*, 1974). Daily CU started were summed
136 from DOY 182 (July 1st) until DOY 365 (December 31st) using the Utah_Model function
137 (ChillR package; Luedeling, 2019).

138 iv) Predicted leaf fall dates (BBCH 97) were computed according to the thermal (LFT) and
139 photothermal (LFPT) models developed by Delpierre *et al.* (2009) and developed in *Quercus*
140 and *Quercus + Fagus*, respectively. Below a critical photoperiod, temperature colder than a
141 threshold, modulated by a photoperiod function in the case of the LFPT model, are summed
142 up to a critical value (Y_{crit}), corresponding to the leaf fall date. Both LFT and LFPT model
143 were computed using the original or a modified set of parameters: $LF(P)T_{ori}$ and $LF(P)T_{mod}$,
144 respectively.

145 v) The dormancy induction state (DS) was computed according to the DORMPHOT model
146 developed in *Betula pubescens* by Caffarra *et al.* (2011a). The two sigmoidal response

147 function to low temperature and photoperiod, respectively interact through sigmoidal
148 functions. The original (DP_{ori}) and two modified (DP_E and DP_L , for early and late,
149 respectively) sets of parameters were used.

150 *Endodormancy release and budburst*

151 Starting from D_{CA} , the sum of CU was modeled according to the inverse of the Richardson
152 function (Richardson *et al.*, 1974) which was defined as the best function predicting
153 endodormancy release dates in walnut trees (Chuine *et al.*, 2016; Charrier *et al.*, 2018).
154 According to the sequential paradigm, the date where $CU(t)$ reaches the critical threshold CU_{crit}
155 (arbitrary chilling units, CU) is the date of endodormancy release (D_{ER}), or the transition
156 between endodormancy and ecodormancy!

$$157 \quad CU(t + 1) = CU(t) + Max(\text{Min}(T_{high} - \theta(t); T_{high} - T_{low}); 0) \quad (2)$$

158 with $CU(t)$, the chilling unit at day t , T_{high} , both the temperature above which CU equals 0 and
159 the amount of CU when temperature equals T_{low} or lower; CU being linear between T_{low} and
160 T_{high} .

161 The ontogenetic development during ecodormancy stage was modeled according to a
162 sigmoid function (Caffarra *et al.*, 2011a). The date when $FU(t)$ reaches the critical threshold
163 FU_{crit} (arbitrary forcing units, FU) is the budburst date (D_{BB}).

$$164 \quad FU(t + 1) = FU(t) + \frac{1}{1 + e^{-slp(\theta(t) - T_{50})}} \quad (3)$$

165 with $FU(t)$, the forcing unit at day t , slp , the slope of the function at the temperature inducing
166 half of the maximal apparent growth rate T_{50} .

167 *Frost hardiness and frost damages*

168 Frost hardiness and subsequent frost damages were computed using a photothermal model
169 developed on *Pinus sylvestris* (Leinonen, 1996) and adapted on *Juglans regia* (Charrier *et al.*,

2018). Shortly, hardening ability (C_R) changes in relation to the different stage of the annual cycle (endodormancy induction, endodormancy release, ecodormancy and growth). During endodormancy and growth stages, C_R was set to 1 and 0, respectively. During endodormancy induction, C_R was either considered gradually increasing from 0 to 1 during the 30 days before the onset of chilling accumulation (Fixed D_{CA}). For simple dynamic D_{CA} , C_R was set to 0 until the threshold was reached (CU_{min} , FF, T_{min} , T_{mean} or Photoperiod). For models describing continuous process, C_R was defined as the ratio between the related variable and its critical threshold (LF, LFPT and DP models). From the interaction between hardening, temperature and photoperiod, a dynamic potential state of hardiness is computed throughout the year. Daily changes in actual frost hardiness (FH) tend to reduce the difference between potential state of hardiness and FH with a temporal lag (see complete description of the model in the original publication). Frost damages are computed on a daily basis through the relation between FH, frost sensitivity (FS, slope at FH) and minimum temperature θ_{min} as:

$$FD = \frac{1}{1 + e^{FS(FH - \theta_{min})}} \quad (4)$$

184 *Model calibration depending on the onset of chilling accumulation*

185 Three different sub-models, namely endodormancy release, ecodormancy release and frost
186 hardiness, were calibrated one after the other, as they were interrelated. To minimize sums of
187 square between observed and predicted values, we used the nls function (Gauss-Newton
188 algorithm), with different sets of starting values at minimum, average and maximum ranges of
189 parameter realistic values.

190 For endodormancy release model, one parameter was optimized: CU_{crit} corresponding to the
191 sum of chilling units to release endodormancy. The other parameters were set to the values
192 defined by Chuine *et al.* (2016). The dataset was split into calibration and validation datasets

193 containing 18 observations from 6 sites and 16 observations from 5 sites, respectively (Table
 194 1).

195 For ecodormancy model, one parameter was optimized: FU_{crit} corresponding to the sum of
 196 forcing units to break buds. The endodormancy model used to predict D_{ER} was the best from
 197 the previous step and the other parameters set to the values described in Charrier *et al.* (2018).
 198 The dataset was split into calibration and validation datasets containing 41 observations from 7
 199 sites and 36 observations from 4 sites, respectively (Table 1).

200 For frost hardiness model, seven parameters were optimized: T_1 , T_2 , NL_1 , NL_2 , δ , τ and
 201 FU_{critR} . The endodormancy and ecodormancy models used to predict D_{ER} and D_{BB} , were the
 202 best from the previous steps and the other parameters set to the values described in Charrier *et*
 203 *al.* (2018). The dataset was split into calibration and validation datasets containing 60
 204 observations (6 winter periods) from 2 sites and 51 observations (5 winter periods) from 5 sites,
 205 respectively (Table 1).

206 The quality of the fit and the predictive ability of the models depending on D_{CA} were assessed
 207 for calibration and validation datasets computing Root Mean Square Error (RMSE) and
 208 Predictive Root Mean Square Error (RMSEP), respectively:

$$209 \quad RMSE(P) = \sqrt{\frac{\sum_{i=1}^n (\hat{y}_i - y_i)^2}{n}} \quad (5)$$

210 with \hat{y}_i the predicted values for an observation I and y_i the observed values for an observation i

211 As the different D_{CA} provided contrasted results among models, we used a composite
 212 performance index defined as :

$$213 \quad PI = \frac{RMSE_{endoD_i}}{\max(RMSE_{endoD})} + \frac{RMSE_{ecoD_i}}{\max(RMSE_{ecoD})} + \frac{RMSE_{FH_i}}{\max(RMSEP_{FH})} + \frac{RMSEP_{endoD_i}}{\max(RMSEP_{endoD})} +$$

$$214 \quad \frac{RMSEP_{ecoD_i}}{\max(RMSEP_{ecoD})} + \frac{RMSEP_{FH_i}}{\max(RMSEP_{FH})} \quad (6)$$

215 **Results**

216 *Effects of D_{CA} on model accuracy*

217 Fixed D_{CA} only had a relatively small effect on the quality of the fit ($12.3 < RMSE_{endoD} <$
218 15.1 days; coefficient of variation $CV = 6.8\%$ for a 153 days range) and the predictive ability
219 of D_{ER} ($8.3 < RMSEP_{endoD} < 11.8$ days; $CV = 11.7\%$). Fixed D_{CA} between DOY 223 (Aug. 11th)
220 and 274 (Oct. 1st) are relatively efficient to simulate CU accumulation with respect to D_{ER} . The
221 effect of various D_{CA} on the prediction of D_{BB} was also relatively low for the quality of the fit
222 ($7.1 < RMSE_{ecoD} < 8.6$ day; $CV = 6.1\%$) and the predictive ability ($6.9 < RMSEP_{ecoD} < 8.1$
223 days; $CV = 4.7\%$). A wider range of fixed D_{CA} , *i.e.* between 223 and 325 (Nov. 21st), similarly
224 performed for D_{BB} prediction. Annual phenological cycle (D_{ER} and D_{BB}) was thus best predicted
225 when D_{CA} was set to DOY 254 (*i.e.* Sep. 11th). For frost hardiness, fixed D_{CA} earlier than DOY
226 305 (Nov. 1st) provided highly efficient fit ($RMSE < 2.0^{\circ}C$). However, the prediction was not
227 accurate enough, as $RMSEP$ was almost twice higher ($3.2 < RMSEP < 3.9^{\circ}C$).

228 The D_{CA} returned by the various dynamic functions were highly different across France:
229 from DOY 182 ± 5 to 312 ± 14 (median \pm SD; Fig. 1A). Four groups of earliness can be defined:
230 very early (T_{min} and photoperiod), early (DP_E , $LFPT_{mod}$, and LFT_{mod}), intermediate (CU_{min}) and
231 late (LFT_{ori} , $LFPT_{ori}$, DP_{ori} , DP_L and FF). All the dynamic D_{CA} computed via different functions
232 exhibited highly significant correlation with mean annual temperature of the site (Fig. 1B-D).

233 Simple temperature thresholds, such as T_{min} or T_{mean} did not provide accurate phenological
234 ($RMSEP > 11.5$ and 8.0 days for D_{ER} and D_{BB} , respectively) nor FH prediction ($RMSEP >$
235 $3.3^{\circ}C$; Tab. 1). The D_{CA} calculated via a photoperiodic threshold was relatively efficient to
236 predict D_{BB} ($RMSEP = 6.8$ days), but not D_{ER} ($RMSEP = 10.2$ days) nor FH ($RMSEP = 3.5^{\circ}C$).

237 The D_{CA} computed using the Utah function did not provide accurate prediction for any
238 variable of interest ($RMSEP = 14.1$ days, 7.8 days and $3.5^{\circ}C$ for D_{ER} , D_{BB} and FH,

239 respectively). The leaf fall thermal function (LFT), using either the original (LFT_{ori}) or the
240 modified sets of parameters (LFT_{mod}), was relatively efficient to predict D_{BB} (RMSEP = 7.23
241 days) but less efficient for D_{ER} and FH (RMSEP ≥ 9.2 and 3.2 for D_{ER} and FH, respectively).
242 The leaf fall photothermal function (LFPT) provided accurate predictions for phenological
243 dates (RMSEP ≤ 8.8 and 6.9 days for D_{ER} and D_{BB} respectively) but not for FH (RMSEP > 3.2
244 °C). The D_{CA} computed using the DORMPHOT function were the most efficient to predict D_{ER},
245 D_{BB} and FH, in the original and ‘Late’ versions of the function (DP_{ori}, and DP_L, respectively).
246 Finally, the performance index (PI) accounting for all the models and methods of computing
247 D_{CA} could not distinguish between DP_{ori} and DP_L (PI = 6.31).

248 Finally, the different processes exhibited contrasted thickness linkage with D_{CA}. For
249 ecodormancy, a wide range of fixed date (100 days range: Aug. 11th until Nov. 21st) and all the
250 computations using photoperiod as an input variable, provided good fit and predictive
251 accuracies (RMSE_{EcoD} and RMSE_{EndoD} lower than 8 and 7.6 days, respectively). Endodormancy
252 release was slightly more restrictive with the best predictions either provided by fixed calendar
253 dates (Aug. 11th until Oct. 1st) or dynamic functions integrating the interaction between
254 temperature and photoperiod (LFPT and DP). Frost hardiness was the most restrictive, with
255 excellent predictive accuracy when using D_{CA} computed by DORMPHOT model (DP_{ori} and
256 DP_L; RMSEP < 3.0°C) compared to all the other computations.

257 Although both DP_{ori} and DP_L performed almost equally for the three variables of interest
258 (D_{ER}, D_{BB} and FH), DP_L exhibited a slightly better correlation to predict the dynamic of Mean
259 Time until budburst (MTB) during the period of dormancy induction (R² = 0.262 and 0.282 for
260 DP_{ori} and DP_L, respectively; Figure 2). Furthermore, as FH was slightly better predicted using
261 DP_L (RMSEP = 2.6°C), D_{CA} predicted by this function was selected to predict the current and
262 future frost risks (Fig. 3).

263 *Predictions under current and future climates*

264 Using D_{CA} computed from DP_L endodormancy release dates under current climate exhibited
265 a structured geographical pattern across France. Endodormancy release dates spanned over a
266 60 days range (Fig. 3A): earlier in mountain area (Early December) and later on the
267 Mediterranean (Mid-February) and southwestern coasts (Late January). Budburst dates
268 exhibited an opposite pattern over a 77 days range (Fig. 3B): from Mid-April in Southern and
269 Western parts until late June in mountainous area. Endodormancy release and budburst dates
270 were highly correlated to mean annual temperature, although through different functions
271 (exponential and cubic function for endodormancy release and budburst, respectively; Fig. 3C-
272 D).

273 The geographic structure was less obvious for frost damages, with very low predicted
274 damages during autumn (Fig. 4A) and spring (Fig. 4C), except in high mountain area. During
275 the winter period, higher frost damages are predicted in the northeastern part of France
276 (Burgundy, Alsace, Lorraine), in mountain areas and in the north of Rhone valley (Fig. 4B).
277 Average predicted damages in autumn and spring were highly correlated to the date of first ($<-$
278 4°C) and last frost event ($< 0^{\circ}\text{C}$), respectively (Fig. 4D; F), whereas maximum winter damages
279 were correlated to absolute annual temperature (Fig. 4E).

280 Similar trends are observed under future climate predictions, with high delay in both the
281 onset of dormancy and release for mean annual temperature higher than 5°C (Fig. 5A, B).
282 However, the delay affecting endodormancy stage does not carry over toward budburst with
283 earlier budburst with increasing temperature for lower mean annual temperature than 10°C (Fig.
284 5C). It should be noted that similar or earlier budburst is likely to happen for higher temperature,
285 and this may be observed in up to one quarter of France at the end of the XXIst century: from 5
286 (RCP 4.5) to 27% (RCP8.5 scenario) of the French territory in 2051-2100 (Fig. 6). Although
287 such a delay is not forecasted within the 'Noix de Grenoble' Protected Designation of Origin
288 area, budburst would be delayed in most of the 'Noix du Périgord' area under RCP8.5 scenario

289 (75.1% 2006-2050 and 94.2% 2051-2100). Overall, frost damages are expected to decrease, on
290 average, all over France (Fig. S1). However, in North East and Massif Central, higher decennial
291 risks are predicted under RCP 2.6 *scenario* (2006-2051; Fig. S2).

292 **Discussion**

293 Defining the initial date for cyclical processes is a critical issue. To predict annual
294 phenological cycle in perennial organisms, such as trees, various empirical rules have been used
295 so far. The onset of chilling accumulation during endodormancy stage (D_{CA}) had, for instance,
296 been arbitrarily set using fixed dates across years and locations (Chuine *et al.*, 2016) or, under
297 the dependence of environmental factors controlling the induction of dormancy (Caffarra *et al.*,
298 2011b). In the current study, we used long-term observations of phenological stages
299 (endodormancy release and budburst) and related processes (frost acclimation and
300 deacclimation) in various environmental conditions and showed that the DORMPHOT model
301 was the most relevant to predict winter biology in walnut trees.

302 Depending on the studied process, not all computation performed equally (Tab. 2). The
303 effect of D_{CA} on ecodormancy and budburst was buffered during endodormancy release. From
304 a budburst perspective, various rules for D_{CA} computation can thus be considered as valid,
305 although they all consider a potential effect of photoperiod, either directly or indirectly via fixed
306 date (Welling *et al.*, 1997; Chuine and Régnière, 2017). A narrower range of fixed date and
307 fewer dynamic computations of D_{CA} (DORMPHOT and LFPT models) provided accurate
308 predictions for endodormancy release dates. However, providing predictive rules only based on
309 one or two phenological stages, even though with a large number of measurements (more than
310 100 dates, combining endodormancy and budburst, in the present study) does not provide
311 sufficient details for continuous process modeling. Introducing frost hardiness as a co-variable
312 of dormancy induction and release provided higher temporal resolution into these concurring

313 processes (Welling & Palva, 2006; Charrier *et al.*, 2011; Hanninen, 2016). Through a multi
314 criterion analysis, the D_{CA} simulated by the DORMPHOT model provided the most accurate
315 predictions. This model, originally developed in *Betula pubescens*, is thus relevant for other
316 deciduous species such as *Juglans regia*. The conceptual development of this model is indeed
317 based on experimental results combining photoperiod and temperature manipulation (Caffarra
318 *et al.*, 2011b), whereas other formalisms were based on empirical observations (*e.g.* leaf fall).
319 Photoperiod and temperature are intimately related in controlling annual weather dynamics.
320 However, temperature fluctuation is much higher at a given date of the year which could induce
321 high variability in the onset of the winter season (see *e.g.* Fig.1). Since dormancy induction and
322 frost acclimation are lengthy processes (*e.g.* ca. 1-2 month), perennial plants cannot only rely
323 on temperature changes that can be too sudden for the onset of winter rest (Caffarra *et al.*,
324 2011a). Both photoperiod and temperature variables thus affect annual phenological cycle in
325 perennial plants, although at different ratio across species. Photoperiod is for instance
326 predominant in *Populus sp* (Kalcsits *et al.*, 2009) and *Vitis sp* (Fennel & Hoover 1991), while
327 temperature in *Malus sp* and *Pyrus sp* (Heide & Prestrud, 2005) and *Sorbus sp* (Heide, 2011).
328 The interaction of both photoperiod and temperature has been showed in *Prunus sp* (Heide
329 2008). Integrating both variables is an interesting strategy to prevent dormancy induction
330 during cold late summer (without frost risks) while maintaining physiological activity under
331 extended warm periods. It has been hypothesized that the modulation of photoperiod sensitivity
332 by temperature may be related by thermal effect on phytochrome perception of day length
333 (Mølmann *et al.*, 2005).

334 The selected rule for D_{CA} , predicting a delayed chilling accumulation in warmer locations
335 ($> 7^{\circ}\text{C}$ MAT; Fig. 1C; 5A) would further delay endodormancy release in such area (Fig. 3 A,
336 C). However, cold weather would limit ontogenetic development during ecodormancy,
337 providing a negative picture of D_{ER} vs D_{BB} (Fig. 3). Under future climatic conditions such as

338 predicted by RCPs *scenarii*, this picture is likely to be blurred as the tipping point for budburst
339 would be achieved (*ca.* 14°C MAT). Below 14°C, endodormancy would be released and
340 warmer temperature of the winter-spring period lead to earlier budburst.

341 Date of first frost (< 0°C), minimum temperature and date of late frost (<-4°C) appear as
342 good proxies to predict early, maximum and late frost damages, respectively (Fig. 4D-F).
343 Predicted minimal temperature are expected to decrease as well and, even though flushing buds
344 would be highly vulnerable to late frost, they are likely not to be exposed to damaging
345 temperature (Fig. 4). Although climate models agree on the average trend, they are still unclear
346 on the climate extreme events such as early and late frost events. Notably, the decennial
347 damages (*i.e.* maximum damage occurring every ten years) may increase in North East and
348 Massif Central area (Fig. S2). The relative balance between photo- and thermosensitivity is
349 likely to be a critical trait explaining this trend. In the near future in these areas, minimum
350 temperature are still likely to happen while dormancy induction and frost acclimation would be
351 delayed by mean temperature increase.

352 Above the 14°C threshold, endodormancy induction and release would be more delayed than
353 ecodormancy hastened, resulting in delayed budburst due to a lack of chilling, compared to the
354 present situation. This situation would cover up to one quarter of France under RCP 8.5 scenario
355 (Fig. 6). Although it would significantly reduce frost damages, even under false spring *scenarii*,
356 lack of chilling would induce severe agronomic troubles such as erratic patterns of blooming,
357 floribondity, and potential dischronism with anthesis. A similar pattern is also expected using
358 fixed date (see Fig S3).

359 With respect to French nuts production, both IGP regions would face distinct threads. In the
360 Périgord, chilling requirements are likely not to be met, and lower chilling varieties have to be
361 selected, as the current ones do not exhibit variability for this trait (Charrier *et al.*, 2011). In
362 Grenoble, earlier budburst dates are expected, leading to higher exposure to frost events, and

363 varieties with higher forcing requirements may help to stabilize the production (Charrier *et al.*,
364 2018). However, both regions seem relatively safe with respect to frost damages.

365 **Conclusions and perspectives**

366 This study highlighted the relevance of dynamic dates for simulating annual phenological
367 cycle and frost acclimation. The DORMPHOT model, integrating temperature and
368 photoperiodic control of dormancy induction, is the most efficient for all studied processes. On
369 one hand, higher decennial damages would be observed in the near future on *ca.* 15% of French
370 territory because of late frost acclimation. On the other hand, the tipping point for phenological
371 processes is likely to be reached during the XXIst century with chilling requirements that are
372 likely not to be fulfilled. The correlation between MAT, phenological stages and frost damages
373 is an important tool, to build relevant meta-models at the global scale.

374

- 376 Arora, R., Rowland, L. J., & Tanino, K. (2003). Induction and release of bud dormancy in
377 woody perennials: a science comes of age. *HortScience*, 38(5), 911-921.
- 378 Balandier, P., Gendraud, M., Rageau, R., Bonhomme, M., Richard, J. P., & Parisot, E. (1993).
379 Bud break delay on single node cuttings and bud capacity for nucleotide accumulation as
380 parameters for endo-and paradormancy in peach trees in a tropical climate. *Scientia*
381 *Horticulturae*, 55(3-4), 249-261.
- 382 Basler, D., & Körner, C. (2012). Photoperiod sensitivity of bud burst in 14 temperate forest tree
383 species. *Agricultural and Forest Meteorology*, 165, 73-81.
- 384 Caffarra, A., Donnelly, A., Chuine, I., & Jones, M. B. (2011a). Modelling the timing of *Betula*
385 *pubescens* budburst. I. Temperature and photoperiod: a conceptual model. *Climate*
386 *Research*, 46(2), 147-157.
- 387 Caffarra, A., Donnelly, A., & Chuine, I. (2011b). Modelling the timing of *Betula pubescens*
388 budburst. II. Integrating complex effects of photoperiod into process-based models. *Climate*
389 *research*, 46(2), 159-170.
- 390 Charrier, G., & Améglio, T. (2011). The timing of leaf fall affects cold acclimation by
391 interactions with air temperature through water and carbohydrate contents. *Environmental*
392 *and Experimental Botany*, 72(3), 351-357.
- 393 Charrier, G., Bonhomme, M., Lacoite, A., & Améglio, T. (2011). Are budburst dates,
394 dormancy and cold acclimation in walnut trees (*Juglans regia* L.) under mainly genotypic or
395 environmental control?. *International journal of biometeorology*, 55(6), 763-774.
- 396 Charrier, G., Chuine, I., Bonhomme, M., & Améglio, T. (2018). Assessing frost damages using
397 dynamic models in walnut trees: exposure rather than vulnerability controls frost risks.
398 *Plant, Cell & Environment*, 41(5), 1008-1021.
- 399 Chuine, I., & Régnière, J. (2017). Process-based models of phenology for plants and animals.
400 *Annual Review of Ecology, Evolution, and Systematics*, 48, 159-182.
- 401 Chuine, I., Bonhomme, M., Legave, J. M., García de Cortázar-Atauri, I., Charrier, G., Lacoite,
402 A., & Améglio, T. (2016). Can phenological models predict tree phenology accurately in the
403 future? The unrevealed hurdle of endodormancy break. *Global Change Biology*, 22(10),
404 3444-3460.
- 405 Delpierre, N., Dufrière, E., Soudani, K., Ulrich, E., Cecchini, S., Boé, J., & François, C. (2009).
406 Modelling interannual and spatial variability of leaf senescence for three deciduous tree
407 species in France. *Agricultural and Forest Meteorology*, 149(6-7), 938-948.
- 408 Dennis, F. G. (2003). Problems in standardizing methods for evaluating the chilling
409 requirements for the breaking of dormancy in buds of woody plants. *HortScience*, 38(3),
410 347-350.
- 411 Déqué, M., Rowell, D. P., Lüthi, D., Giorgi, F., Christensen, J. H., Rockel, B., ... & van den
412 Hurk, B. J. J. M. (2007). An intercomparison of regional climate simulations for Europe:
413 assessing uncertainties in model projections. *Climatic Change*, 81(1), 53-70.
- 414 Fennell, A., & Hoover, E. (1991). Photoperiod influences growth, bud dormancy, and cold
415 acclimation in *Vitis labruscana* and *V. riparia*. *Journal of the American Society for*
416 *Horticultural Science*, 116(2), 270-273.
- 417 Ferguson, J. C., Tarara, J. M., Mills, L. J., Grove, G. G., & Keller, M. (2011). Dynamic thermal
418 time model of cold hardiness for dormant grapevine buds. *Annals of botany*, 107(3), 389-
419 396.
- 420 Gauzere, J., Lucas, C., Ronce, O., Davi, H., & Chuine, I. (2019). Sensitivity analysis of tree
421 phenology models reveals increasing sensitivity of their predictions to winter chilling
422 temperature and photoperiod with warming climate. *Ecological Modelling*, 411, 108805.

423 Hänninen, H., & Tanino, K. (2011). Tree seasonality in a warming climate. *Trends in plant*
424 *science*, 16(8), 412-416.

425 Hänninen, H. (2016). Boreal and temperate trees in a changing climate. *Dordrecht: Springer.*
426 *doi*, 10, 978-94.

427 Heide, O. M., & Prestrud, A. K. (2005). Low temperature, but not photoperiod, controls growth
428 cessation and dormancy induction and release in apple and pear. *Tree physiology*, 25(1),
429 109-114.

430 Heide, O. M. (2008). Interaction of photoperiod and temperature in the control of growth and
431 dormancy of *Prunus* species. *Scientia Horticulturae*, 115(3), 309-314.

432 Heide, O. M. (2011). Temperature rather than photoperiod controls growth cessation and
433 dormancy in *Sorbus* species. *Journal of experimental botany*, 62(15), 5397-5404.

434 Kalcsits, L. A., Silim, S., & Tanino, K. (2009). Warm temperature accelerates short
435 photoperiod-induced growth cessation and dormancy induction in hybrid poplar (*Populus*×
436 spp.). *Trees*, 23(5), 971-979.

437 Landsberg, J. J. (1974). Apple fruit bud development and growth; analysis and an empirical
438 model. *Annals of Botany*, 38(5), 1013-1023.

439 Lang, G. A., Early, J. D., Martin, G. C., & Darnell, R. L. (1987). Endo-, para-, and
440 ecodormancy: physiological terminology and classification for dormancy research.
441 *HortScience*, 22(3), 371-377.

442 Leinonen, I. (1996). A simulation model for the annual frost hardiness and freeze damage of
443 Scots pine. *Annals of Botany*, 78(6), 687-693.

444 Luedeling, E. (2019) Statistical Methods for Phenology Analysis in Temperate Fruit Trees,
445 chillR Package.

446 Mauget, J. C., (1980). Dormance et précocité de débourrement des bourgeons chez quelques
447 cultivars de Noyer (*Juglans regia* L.).

448 Maurya, J. P., & Bhalerao, R. P. (2017). Photoperiod-and temperature-mediated control of
449 growth cessation and dormancy in trees: a molecular perspective. *Annals of botany*, 120(3),
450 351-360.

451 Mølmann, J. A., Asante, D. K., Jensen, J. B., Krane, M. N., Ernstsén, A., Junttila, O., & Olsen,
452 J. E. (2005). Low night temperature and inhibition of gibberellin biosynthesis override
453 phytochrome action and induce bud set and cold acclimation, but not dormancy in PHYA
454 overexpressors and wild-type of hybrid aspen. *Plant, Cell & Environment*, 28(12), 1579-
455 1588.

456 Rageau, R. (1982). Etude expérimentale des lois d'action de la température sur la croissance
457 des bourgeons floraux du pêcher (*Prunus persica* L. Batsch) pendant la postdormance.

458 Réaumur, R. A. F. d. 1735. Observations du thermomètre, faites à Paris durant l'année 1735,
459 comparées avec celles qui ont été faites sous la ligne, à l'isle de France, à Alger et quelques
460 unes de nos isles de l'Amérique. Mémoires de l'Académie des Sciences de Paris.

461 Repo, T., & Lappi, J. (1989). Estimation of standard error of impedance-estimated frost
462 resistance. *Scandinavian Journal of Forest Research*, 4(1-4), 67-74.

463 Richardson, E. A., EA, R., SD, S., & DR, W. (1974). A model for estimating the completion of
464 rest for "Redhaven" and "Elberta" peach trees.

465 Vegis, A. (1964). Dormancy in higher plants. *Annual review of plant physiology*, 15(1), 185-
466 224.

467 Weinberger, J. H. (1950). Chilling requirements of peach varieties. In *Proceedings. American*
468 *Society for Horticultural Science* (Vol. 56, pp. 122-8).

469 Weinberger, J. H. (1956). Prolonged dormancy trouble in peaches in the southeast in relation
470 to winter temperatures. *Journal of the American Society for Horticultural Science*, 67, 107-
471 112.

- 472 Weinberger, J. H. (1967). Some temperature relations in natural breaking of the rest of Peach
473 flower buds in the San Joaquin Valley, California. *Proceedings of the American Society for*
474 *Horticultural Science*, 51, 84-89.
- 475 Welling, A., & Palva, E. T. (2006). Molecular control of cold acclimation in trees. *Physiologia*
476 *Plantarum*, 127(2), 167-181.
- 477 Welling, A., Kaikuranta, P., & Rinne, P. (1997). Photoperiodic induction of dormancy and
478 freezing tolerance in *Betula pubescens*. Involvement of ABA and dehydrins. *Physiologia*
479 *Plantarum*, 100(1), 119-125.
- 480 Welling, A., Moritz, T., Palva, E. T., & Junttila, O. (2002). Independent activation of cold
481 acclimation by low temperature and short photoperiod in hybrid aspen. *Plant Physiology*,
482 129(4), 1633-1641.
- 483 Zhang, M. I. N., & Willison, J. H. M. (1987). An improved conductivity method for the
484 measurement of frost hardiness. *Canadian Journal of Botany*, 65, 710–715.
- 485

486 **Acknowledgements**

487 The author wants to acknowledge the essential contribution of Marc Bonhomme, Aline Faure,
488 Jean-Claude Mauget, Remi Rageau, Jean-Pierre Richard for dormancy release date
489 measurements. Phenological data and stem materials were provided by Neus Aleita, Romain
490 Baffoin, Fabrice Lheureux, Marianne Naudin and Eloise Tranchand. The author is also thankful
491 to Thierry Améglio, André Lacointe and Heikki Hanninen for constructive comments on
492 preliminary versions of the manuscript. Part of the collected data were supported by the Pôle
493 National de Données de la Biodiversité (a.k.a SOERE Tempo).
494

495 **Figure captions**

496 **Figure 1. A** Distribution of date at the onset of chilling accumulation T_0 across France over the 1950-2005 period according to different
497 computations: T_{min} minimum temperature (lower than 15.28°C), DP DORMPHOT model from different sets of parameters (O: original,
498 E early, L Late), LFT_{mod} Leaf Fall model (thermal version modified), LFPT Leaf Fall model Photothermal version Original and modified.
499 B, C and D T_0 depending on mean annual temperature.

500 **Figure 2** MTB depending on Day after September 1st (A), DS according to DP_{ori} (B), DS according to DP_L (C).

501 **Figure 3. A-B.** Average dates of endodormancy release (A) and budburst (B) predicted across France under current climatic
502 conditions. **C-D.** Average dates of endodormancy release (C) and budburst (D) depending on mean annual temperature (°C) across
503 France.

504 **Figure 4. A-C.** Average frost damages predicted across France under current climatic conditions in autumn (A), winter (B) and
505 spring (C). **D.** Average early frost damages depending on the average date of the first frost lower than 0°C. **E.** Average maximum
506 frost damages depending on the average annual minimum temperature. **F.** Average late frost damages depending on the average
507 date of the last frost lower than -4°C.

508 **Figure 5. A-C.** Average date of onset of dormancy (A), endodormancy release (B), budburst (C) over France depending on the
509 mean annual temperature under current climate (gray), RCP 2.6 (2006-2051 cyan, 2051-2100 blue), RCP 4.5 (2006-2051 green,
510 2051-2100 yellow), and RCP 8.5 *scenarii* (2006-2051 purple, 2051-2100 red). **D.** Average predicted autumn early frost damages
511 depending on the date of first frost (<0°C) **E.** Average predicted maximum winter frost damages depending on the mean absolute
512 minimum temperature **F.** Average predicted spring late frost damages depending on the date of last frost (<-4°C). Each dot
513 represent the average of the considered period at 8 x 8km spatial resolution, black line represent the best non-linear regression.

514 **Figure 6.** Relative change in predicted average budburst date across France according to different climatic *scenarii* and time periods
515 (earlier and later budburst dates than the mean are represented in blue and red, respectively).

516

517

518 **Table 1.** Site and dataset description

Location	Elevation (m asl.)	Latitude °	Longitude °	Mean annual temperature (°C)	Minimum temperature (°C)	Absolute minimum temperature (°C)	Number of freezing events	First Frost (Autumn) DOY	Last Frost (Spring) DOY	Number of observations (years and number of dates in brackets)					
										Endodormancy Release		Budburst		Frost Hardiness	
										Calibration	Validation	Calibration	Validation	Calibration	Validation
Balandran	69	43.758	4.516	16.90	12.00	-3.78	14.5	340	50	1	1	0	0	0	0
Chatte	304	45.143	5.282	13.62	8.15	-9.39	61.7	308	102	0	0	12	11	0	1 (6)
Creyse	115	44.887	1.597	14.65	8.52	-8.50	52.4	309	104	0	0	13	12	0	1 (8)
Crouël	340	45.779	3.142	13.25	9.26	-11.51	59.6	302	108	13	12	4	4	5 (49)	2 (21)
Orcival	1150	45.683	2.842	12.92	7.72	-12.13	97.4	291	126	1	1	1	0	0	0
Terrasson	90	45.136	1.300	14.61	8.96	-9.69	47.4	311	100	1	1	1	0	0	0
Theix	945	45.706	3.021	9.70	6.22	-15.11	100.3	282	129	1	1	1	0	1 (11)	1 (9)
Toulenne	22	44.557	-0.263	15.38	10.56	-6.09	25.9	325	74	1	0	9	9	0	0
Mas Bové	112	41.170	1.169	15.87	10.81	-4.05	14.9	343	47	0	0	0	0	0	1 (7)

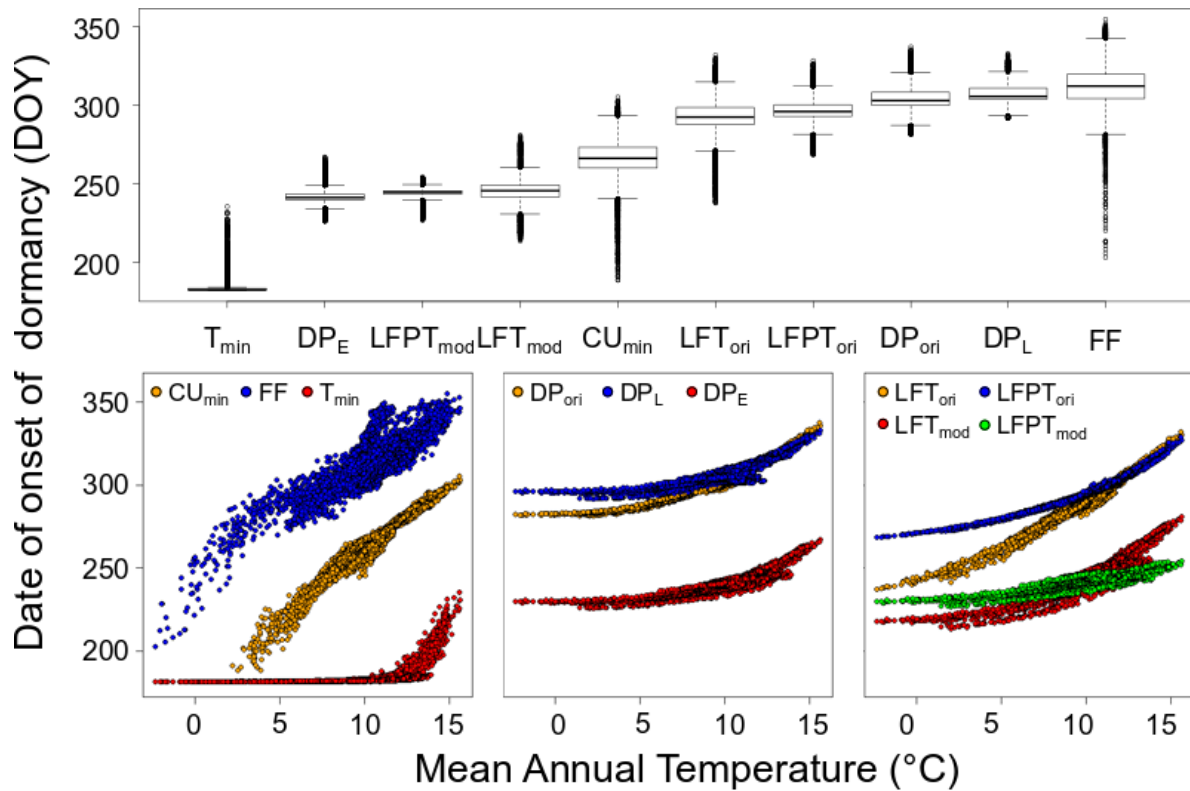
519

520

521 **Table 2.** Quality assessment of different models. RMSE(P) less than 15% higher than minimum RMSE or RMSEP are indicated in
 522 bold.

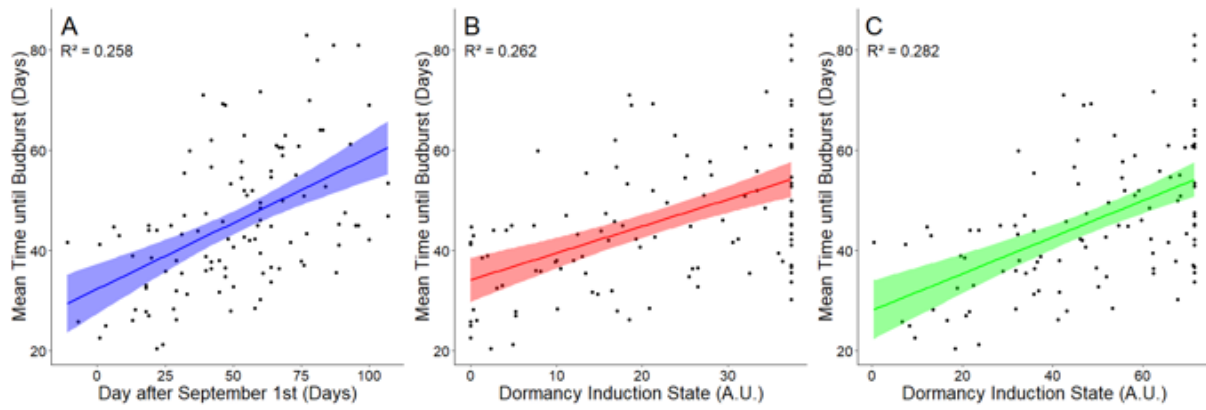
			Endodormancy	Budburst		Frost		PI	
			Release Date		Date		Hardiness		
Type	Function	D _{CA}	RMSE	RMSEP	RMSE	RMSEP	RMSE	RMSEP	
			(days)	(days)	(days)	(days)	(°C)	(°C)	
Fixed		182 (Jul. 1 st)	12.84	11.84	8.58	8.08	1.79	3.52	7.31
		192 (Jul. 11 th)	12.64	11.48	8.44	7.57	1.79	3.39	7.10
		202 (Jul.21 st)	12.41	10.73	8.25	7.28	1.80	3.42	6.94
		213 (Aug. 1 st)	12.33	10.06	8.06	7.14	1.79	3.46	6.81
		223 (Aug. 11 th)	12.65	9.36	7.78	6.89	1.78	3.49	6.68
		233 (Aug. 21 st)	12.68	8.71	7.61	6.85	1.78	3.49	6.58
		244 (Sep. 1 st)	12.87	8.75	7.39	7.03	1.79	3.48	6.59
		254 (Sep. 11 th)	13.19	8.49	7.26	6.88	1.77	3.47	6.53
		264 (Sep. 21 st)	13.70	8.80	7.15	7.24	1.74	3.24	6.55
		274 (Oct. 1 st)	13.80	8.47	7.25	7.38	1.73	3.29	6.56
		284 (Oct. 11 th)	13.98	8.29	7.10	6.93	1.77	3.37	6.52
		294 (Oct. 21 st)	14.39	8.47	7.25	7.15	1.84	3.30	6.64
		305 (Nov. 1 st)	14.48	9.22	7.45	7.47	1.84	3.21	6.78
		315 (Nov. 11 th)	14.48	9.93	7.52	7.56	2.15	3.42	7.16
		325 (Nov. 21 st)	14.67	10.26	7.46	7.43	2.90	3.90	7.81
	335 (Dec. 1 st)	15.10	10.33	7.58	7.67	3.77	3.52	8.77	
Dynamic	Simple	FF	17.71	14.15	9.35	15.69	1.90	4.92	9.84
		T _{min}	12.88	11.93	8.55	8.03	1.79	3.37	7.25
		T _{mean}	12.93	11.59	8.70	8.47	1.81	3.38	7.31
		Photoperiod	12.31	10.24	7.94	6.85	1.80	3.46	6.78
	Complex	CU _{min}	16.32	14.08	8.22	7.78	1.78	3.48	7.74
		LFT _{ori}	12.91	10.37	8.11	7.23	1.76	3.22	6.81
		LFT _{mod}	12.57	9.16	8.11	7.23	1.80	3.19	6.83
		LFPT _{ori}	13.34	8.67	7.42	6.72	1.83	3.24	6.51
		LFPT _{mod}	12.66	8.81	7.43	6.89	1.78	3.50	6.57
		DP _{ori}	13.01	8.81	7.47	6.61	1.76	2.87	6.31
DP _E		12.05	8.64	7.73	7.24	1.80	3.95	6.77	
DP _L	12.51	9.43	7.52	7.14	1.70	2.65	6.31		

523



524
 525
 526
 527
 528
 529
 530
 531
 532

Figure 1. A Distribution of date at the onset of chilling accumulation (D_{CA}) across France over the 1950-2005 period according to different computations: T_{min} minimum temperature (lower than 15.28°C), DP DORMPHOT model from different sets of parameters (O: original, E early, L Late), LFT_{mod} Leaf Fall model (thermal version modified), LFPT Leaf Fall model Photothermal version Original and modified. B, C and D T0 depending on mean annual temperature.

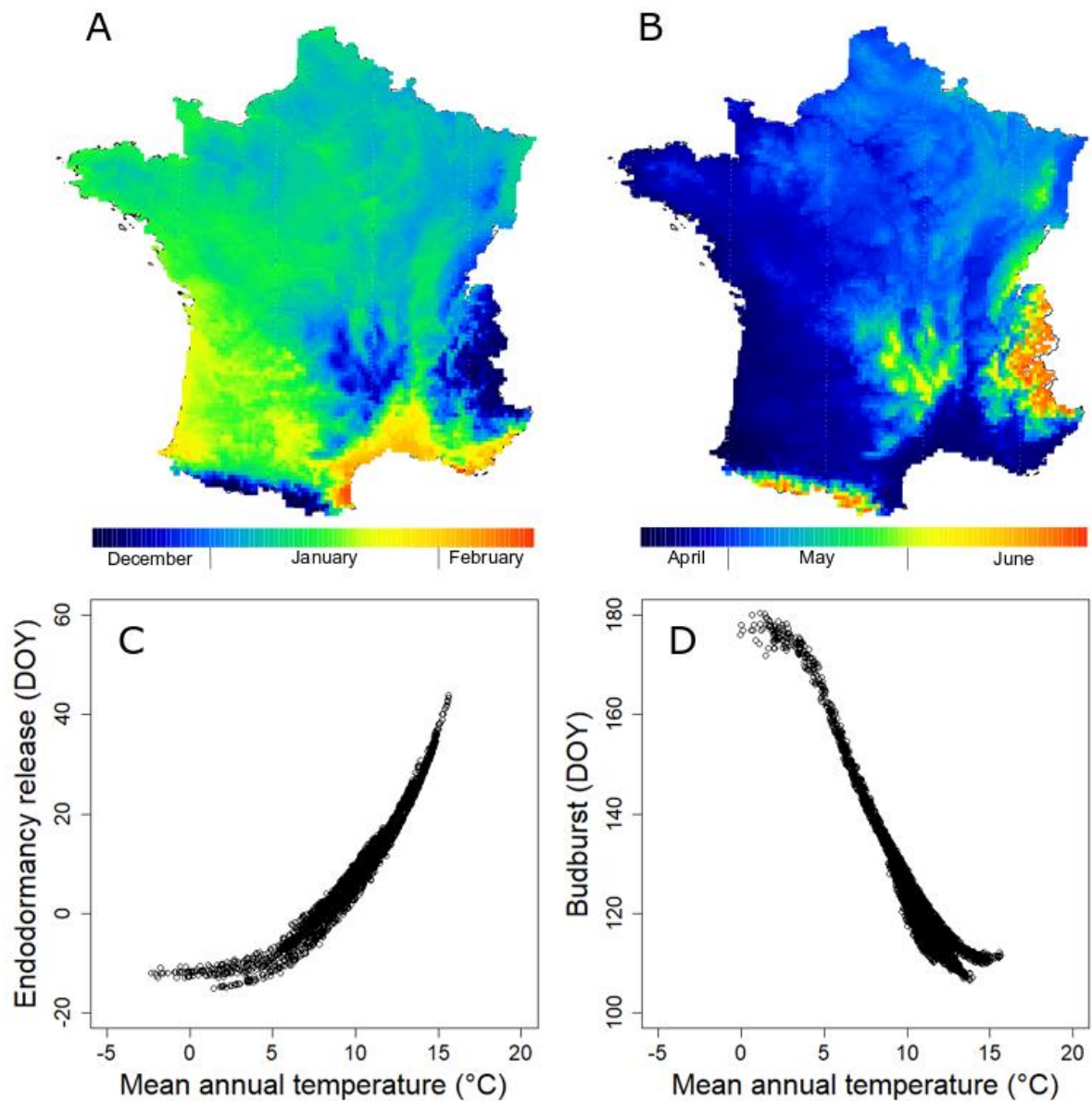


533

534

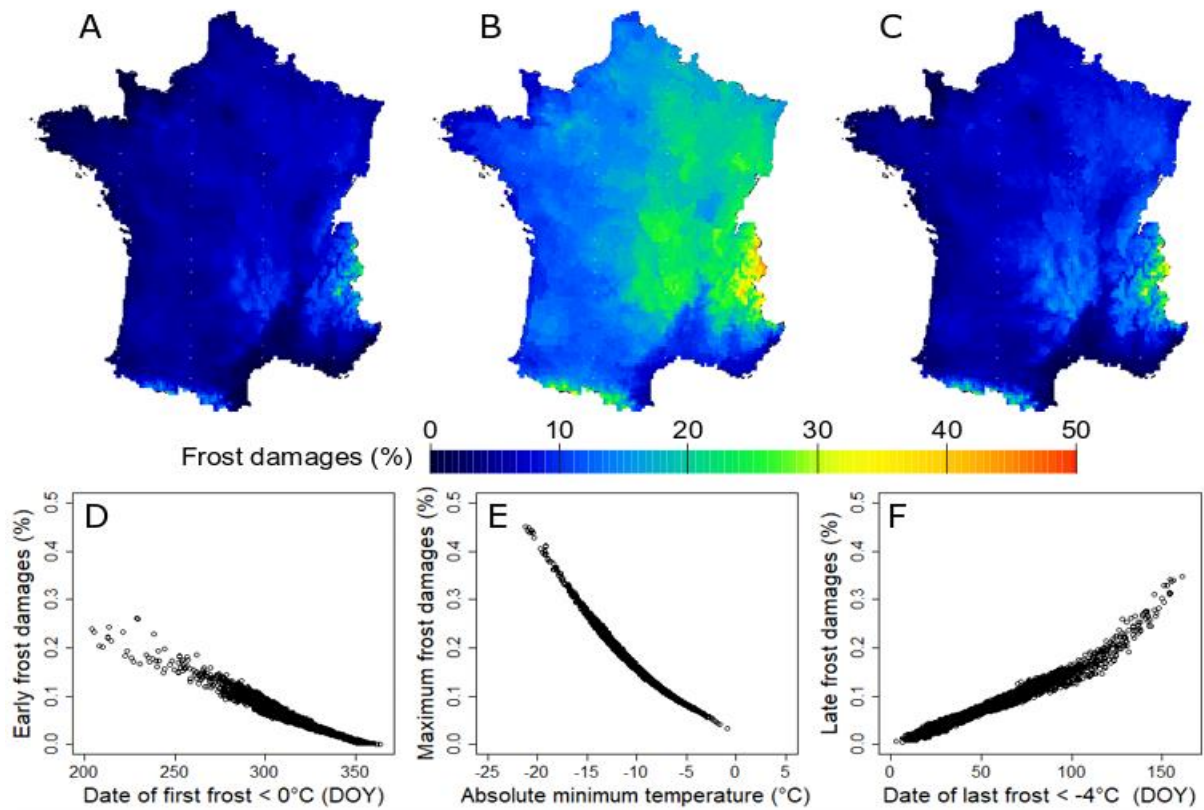
535

Figure 2. Mean time until budburst in forcing test depending on Day after September 1st (A), DS according to DP_{ori} (B), DS according to DP_L (C).



536

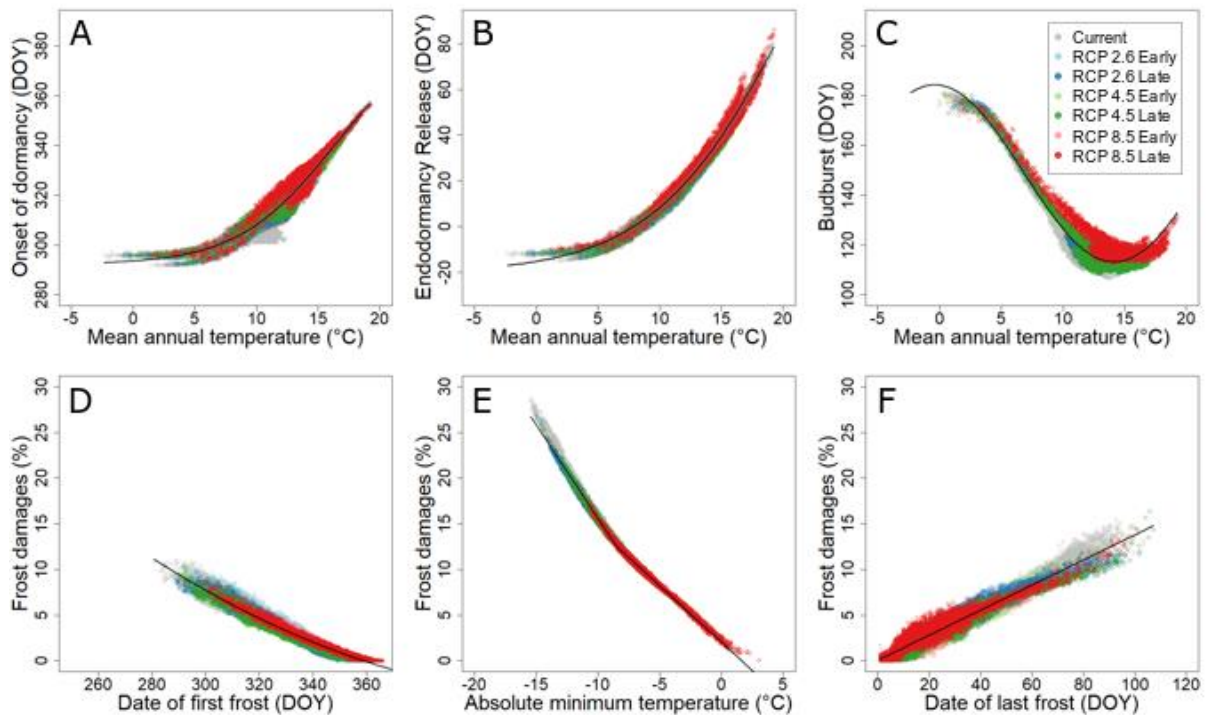
537 **Figure 3. A-B.** Average dates of endodormancy release (A) and budburst (B) predicted
 538 across France under current climatic conditions. **C-D.** Average dates of endodormancy
 539 release (C) and budburst (D) depending on mean annual temperature (°C) across
 540 France.



541

542 **Figure 4. A-C.** Average frost damages predicted across France under current climatic
 543 conditions in autumn (A), winter (B) and spring (C). **D.** Average early frost damages
 544 depending on the average date of the first frost lower than 0°C. **E.** Average maximum
 545 frost damages depending on the average annual minimum temperature. **F.** Average
 546 late frost damages depending on the average date of the last frost lower than -4°C.

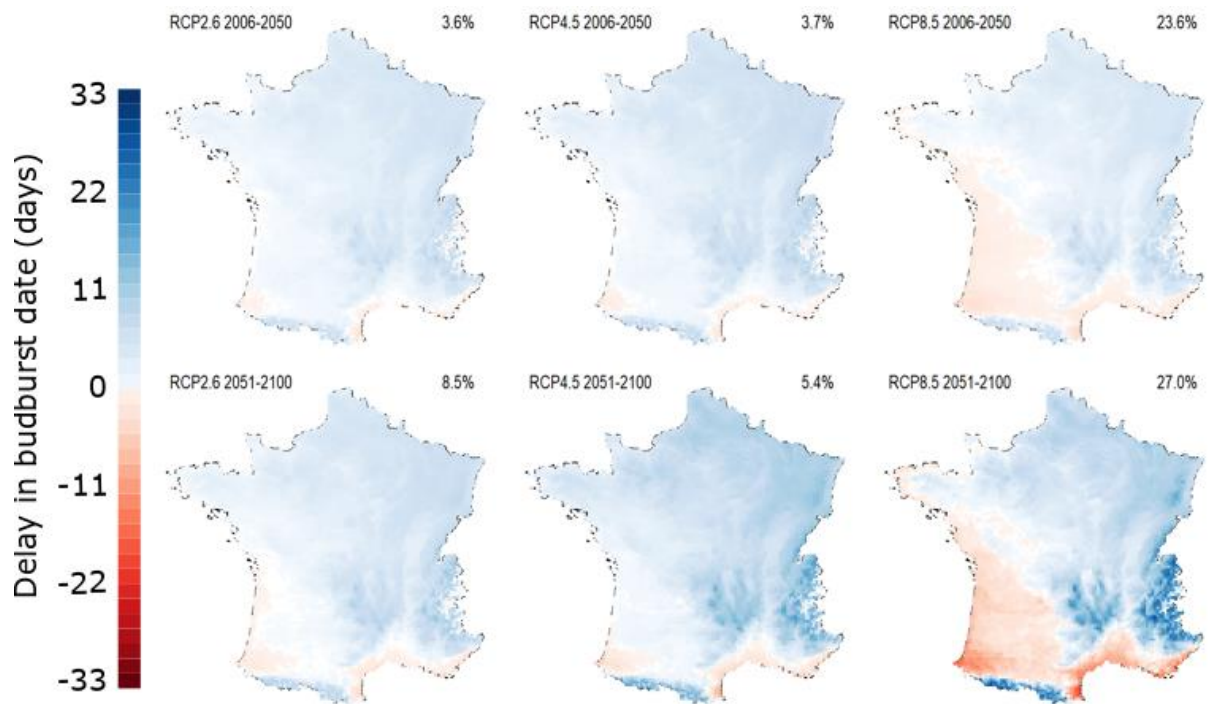
547



548

549 **Figure 5. A-C.** Average date of onset of dormancy (A), endodormancy release (B),
 550 budburst (C) over France depending on the mean annual temperature under current
 551 climate (gray), RCP 2.6 (2006-2051 cyan, 2051-2100 blue), RCP 4.5 (2006-2051
 552 green, 2051-2100 yellow), and RCP 8.5 *scenarii* (2006-2051 purple, 2051-2100 red).
 553 **D.** Average predicted autumn early frost damages depending on the date of first frost
 554 (<0°C) **E.** Average predicted maximum winter frost damages depending on the mean
 555 absolute minimum temperature **F.** Average predicted spring late frost damages
 556 depending on the date of last frost (<-4°C). Each dot represent the average of the
 557 considered period at 8 x 8km spatial resolution, black line represent the best non-linear
 558 regression.

559



560

561 **Figure 6** Relative change in predicted average budburst date across France according
 562 to different climatic *scenarii* and time periods. Earlier and later budburst dates than the
 563 mean are represented in blue and red, respectively). The proportion of area showing
 564 delayed budburst is indicated for each map.

565